Color signals in the primary visual cortex of marmosets

Péter Buzás
National Vision Research Institute of Australia, Carlton, Australia, Department of Optometry and Vision Sciences, The University of Melbourne, Parkville, Australia, & Institute of Physiology, Medical School, University of Pécs, Hungary

Brett A. Szmajda
National Vision Research Institute of Australia, Carlton, Australia, & Department of Optometry and Vision Sciences, The University of Melbourne, Parkville, Australia

Maziar Hashemi-Nezhad
Discipline of Anatomy and Histology, School of Medical Sciences, The University of Sydney, Australia

Bogdan Dreher
Discipline of Anatomy and Histology, School of Medical Sciences, The University of Sydney, Australia

Paul R. Martin
National Vision Research Institute of Australia, Carlton, Australia, & Department of Optometry and Vision Sciences, The University of Melbourne, Parkville, Australia

This study concerns the input from short-wavelength sensitive (S) cone photoreceptors to the primary visual cortex (striate cortex, Brodmann area 17, area V1) in marmosets. Signals from S-cones are thought to reach V1 by way of the koniocellular layers of the dorsal lateral geniculate nucleus. However, it is not known whether the S-cone afferent signals cause selective activation of cytochrome oxidase-rich cortical "blob" domains. To address this question, intrinsic optical signals and extracellular responses of V1 neurons were recorded. Stimuli consisted of drifting achromatic gratings and gratings that stimulated selectively either the S-cones or the medium-long wavelength sensitive (ML) cones. All stimuli produced contrast-dependent activation throughout the imaged regions of V1. The S- and ML-cone-selective stimuli produced activation levels of respectively 30% and 80% of that to achromatic gratings. No spatial variation in the strength of S-cone activation was apparent, and the ratio of S to ML activation was constant across all imaged regions. Consistently, in all of the single neurons recorded from V1, the functional input from S-cones was weaker than the input from ML-cones. We conclude that in the primary visual cortex of marmosets, S-cone signals are uniformly distributed.

Keywords: color vision, parvocellular, koniocellular, magnocellular

Citation: Buzás, P., Szmajda, B. A., Hashemi-Nezhad, M., Dreher, B., & Martin, P. R. (2008). Color signals in the primary visual cortex of marmosets. *Journal of Vision, 8*(10):7, 1–16, http://journalofvision.org/8/10/7/, doi:10.1167/8.10.7.

Introduction

Trichromatic color vision depends on cone photoreceptors with peak spectral sensitivity in the short (S or "blue"), medium (M or "green"), and long (L or "red") regions of the visible spectrum. The signals from S-cones are segregated to distinct retinal pathways and are thought to reach the primary visual cortex by way of specialized relay neurons in the koniocellular layers of the dorsal lateral geniculate nucleus (Chatterjee & Callaway, 2003; Hendry & Reid, 2000; Martin, White, Goodchild, Wilder,

doi: 10.1167/8.10.7 Received November 1, 2007; published October 22, 2008 ISSN 1534-7362 © ARVO

& Sefton, 1997; Szmajda, Buzás, Fitzgibbon, & Martin, 2006). By contrast, relay neurons in the parvocellular and magnocellular layers of macaque and marmoset monkeys receive predominantly M- and L-cone input (Hashemi-Nezhad, Blessing, Dreher, & Martin, 2008; Sun, Smithson, Zaidi, & Lee, 2006), and most parvocellular neurons in trichromatic primates show red-green color opponent properties (reviewed by Solomon & Lennie, 2005).

The parallel retino-geniculate afferent streams to primary visual cortex thus carry distinct spectral signatures, but the distribution of color signals in the primary visual cortex remains poorly understood. Some single-cell recording studies report specific inhibitory ("cone-opponent") contribution of S-cones to color-selective cortical neurons (Cottaris & De Valois, 1998; Sato, Katsuyama, Tamura, Hata, & Tsumoto, 1994), whereas others report mixed excitatory/inhibitory or only weak excitatory S-cone inputs to most V1 cells (Conway & Livingstone, 2006; Horwitz, Chichilnisky, & Albright, 2005; Johnson, Hawken, & Shapley, 2004; Solomon & Lennie, 2005). Functional imaging studies disagree on the extent to which red-green and blue-yellow color signals are segregated to distinct cortical domains (Landisman & Ts'o, 2002a, 2002b; Roe, Fritsches, & Pettigrew, 2005; Xiao, Casti, Xiao, & Kaplan, 2007), and the question whether specific clusters of color-selective neurons are segregated in cytochrome-oxidase-rich "blob" regions remains controversial (Leventhal, Thompson, Liu, Zhou, & Ault, 1995; Livingstone & Hubel, 1984; Lu & Roe, 2008; Roe & Ts'o, 1999; Tootell, Nelissen, Vanduffel, & Orban, 2004; Tootell, Silverman, Hamilton, De Valois, & Switkes, 1988; Ts'o & Gilbert, 1988). Chatterjee and Callaway (2003) recorded signals from S-cone geniculocortical afferents in superficial layers 3B and 4A, consistent with their postulated termination in blob regions. By contrast, the signals from off-type S-cone afferents were encountered lower in layer 4A in a patchy pattern (Chatterjee & Callaway, 2003). How these afferent inputs influence the distribution of color signals in cortical responses is the question addressed by the current study.

The M and L receptors diverged relatively recently in the evolutionary history of primates to yield trichromatic color vision from a primordial, dichromatic, system common to most diurnal mammals (reviewed by Jacobs, 1993; Mollon, 1989; Nathans, 1999). Here, we have studied color responses in the cortex of dichromatic marmosets. These animals possess (in addition to S-cones) only one cone type in the medium-long (ML) wavelength sensitivity range. The segregation of S-cone signals (blue-on and blue-off) to the koniocellular layers has been most clearly demonstrated in marmosets (Hashemi-Nezhad et al., 2008; Martin et al., 1997; Szmajda et al., 2006), largely because in marmoset there is a clear anatomical segregation of koniocellular layers from the magnocellular and parvocellular layers. Furthermore, the organization of koniocellular projections to primary visual cortex appears to be well conserved between New World and Old World monkeys (Casagrande, Yazar, Jones, & Ding, 2007; Fitzpatrick, Itoh, & Diamond, 1983; Livingstone & Hubel, 1984; Solomon, 2002). Given the relative paucity of data on the segregation of color signals in macaque lateral geniculate nucleus (Hendry & Reid, 2000; Hubel & Livingstone, 1990), this makes marmosets an ideal species to study the organization of the primordial S-cone pathway for color vision. We measured the contribution of S-cone signals to individual neurons (by single cell recording) and to the overall activity in primary visual cortex (by intrinsic optical signal imaging). Stimuli were high-contrast gratings that produced specific isolation of the ML- and S-cones. The employment of high contrast cone-selective stimuli allows measurement of absolute (signal *versus* baseline) rather than differential signals as commonly reported in previous optical imaging studies. We addressed two specific questions: firstly, whether S-cone signals combine additively with ML-cone signals in primary visual cortex, and secondly, whether S-cone signals show spatial segregation across the cortical surface.

To our knowledge, so far the effect of colored stimuli was measured in one imaging study of marmoset primary visual cortex (Roe et al., 2005). These authors did not specifically address the nature and distribution of S-cone signals using cone-selective stimuli, as we do here. We show that modulation of S-cones produces significant activation in V1, but the activity shows little sign of spatial non-homogeneity or "patchiness." Rather at each point in the cortex the effect of S-cone modulation is positively correlated with the effect of ML-cone modulation. Furthermore, the response amplitude of the intrinsic signal for achromatic contrast is consistent with additive input from S- and ML-cones. Finally, the V1 neurons whose responses we measured received only weak functional input from S-cones. These results suggest that there is no specific tangential clustering of S-cone-driven activity in marmoset V1.

Methods

Data were obtained from eight adult marmosets (*Callithrix jacchus,* seven male, one female) supplied by the Australian National Health and Medical Research Council (NHMRC) combined breeding facility. Procedures conform to the provisions of the Australian NHMRC code of practice for the use and care of animals and were approved by the institutional animal care and ethics committee. The cone opsin encoding genes of three of the animals were identified by PCR-restriction fragment length polymorphism (Blessing, Solomon, Hashemi-Nezhad, Morris, & Martin, 2004). The genetic predictions were confirmed by single-cell recordings from the dorsal lateral geniculate nucleus as described below.

Animals were anesthetized with inhaled isoflurane (Forthane, Abbott, Sydney, Australia, 1.5–2%) and

intramuscular ketamine (Ketalar, Parke-Davis, Sydney, 30 $mg{\cdot}kg^{-1}$) for surgery. A femoral vein and the trachea were cannulated. Animals were artificially respired with a 70%:30% mixture of NO_2:Carbogen (5% CO_2 in O_2). A venous infusion of 40 $\mu g{\cdot}kg^{-1}$ alcuronium chloride (Alloferin, Roche, Sydney) in dextrose Ringer solution (Baxter, Sydney) was infused at a rate of 1 $ml{\cdot}hr^{-1}$ to maintain muscular relaxation. Anesthesia was maintained during recording with a venous infusion of sufentanil citrate (Sufenta-Forte; 4–10 $\mu g{\cdot}kg^{-1}{\cdot}hr^{-1}$). Electroencephalogram (EEG) and electrocardiogram signals were monitored to ensure adequate depth of anesthesia. The EEG signal was subjected to Fourier analysis. Dominance of low frequencies (1–5 Hz) in the EEG recording and absence of EEG changes under noxious stimulus (tail-pinch) were taken as the chief sign of an adequate level of anesthesia. We found that low anesthetic dose rates in the range cited above were always very effective during the first 24 hours of the experiment; drifts towards higher frequencies (5–10 Hz) in the EEG record thereafter were counteracted by increasing the rate of venous infusion and/or concentration of sufentanil citrate in the infused solution.

The corneas were protected using oxygen permeable contact lenses. The positions of the optic disks and foveae were mapped on a tangent screen positioned 114 cm in front of the animal using a fundus camera equipped with a rear-projection device. The typical duration of a recording session was 48–72 hours. At the termination of the recording session the animal was killed with an overdose of pentobarbitone sodium (80–150 $mg{\cdot}kg^{-1}$, i.v.). The brain was perfused with 4% paraformaldehyde in phosphate buffer then frozen-sectioned in the coronal plane for reconstruction of electrode recording positions (Szmajda et al., 2006). Some sections in three of the animals studied were also reacted for the mitochondrial enzyme cytochrome oxidase as described elsewhere (Solomon, 2002; Wong-Riley, 1979). To illustrate the tangential pattern of blobs, a cytochrome oxidase reacted horizontal section of a flattened cortex preparation is shown in Figure 1; this preparation was from a female marmoset (case MY 116) additional to those studied here.

Optical imaging and single-cell recording of V1 cells were carried out in different animals. In all animals we also recorded responses of dorsal lateral geniculate neurons; results of some of these recordings have been

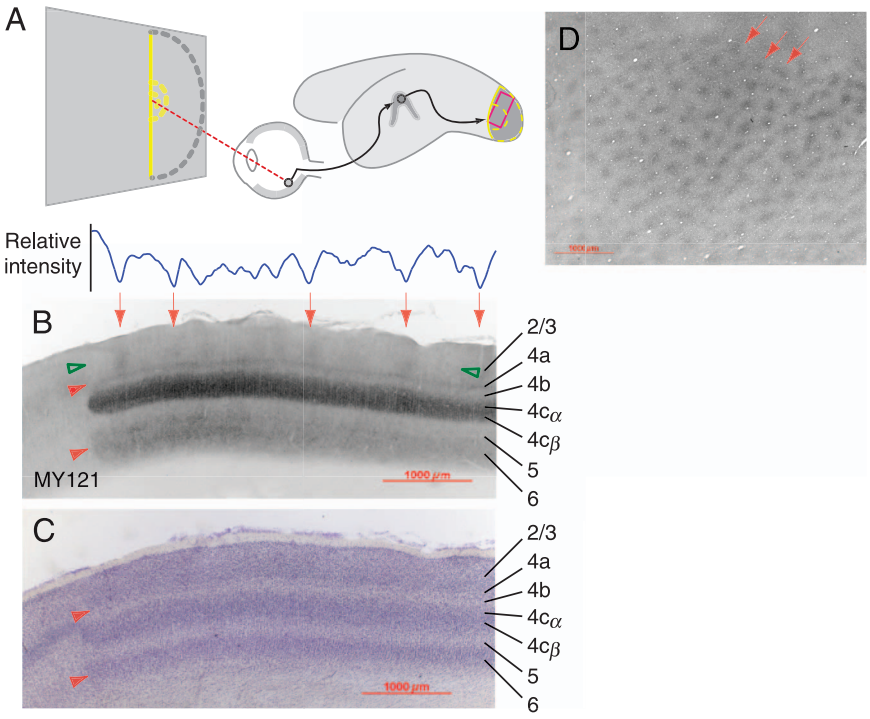

Figure 1. Anatomy of V1 in marmosets. (A) Schematic diagram of the marmoset eye and brain showing the approximate representation of the fovea (1 deg), the central five degrees (yellow dashed lines), and the vertical meridian (solid yellow line) on the lateral aspect of the posterior occipital cortex. Brain schematic modified from Fritches and Rosa (1996). The approximate location of the target region for optical imaging experiments is shown by the magenta rectangle. (B) Coronal section through cytochrome oxidase-reacted section through the foveal representation of V1 at the border with area V2. A dense continuous band of staining in layer 4c and weaker continuous bands in layer 6 and layer 4a (filled arrowhead) are apparent. A weak, interrupted band of staining ("blobs") in layers 2 and 3 is also present (arrows). The trace above the section shows the relative pixel intensity along the trajectory indicated by the open green arrowheads. Intensity dips corresponding to putative blobs are shown. (C) Neighboring Nissl-stained section with cortical laminae labeled according to Brodmann's scheme. (D) Image of flattened cortex (from case MY 116) reacted for cytochrome oxidase. The regular blob pattern in V1 is readily appreciated in such tangential sections; three examples are indicated by arrows.

reported elsewhere (Blessing et al., 2004; Forte, Blessing, Buzás, & Martin, 2006; Hashemi-Nezhad et al., 2008). These recordings allowed us to identify the ML-cone type present in each animal (Blessing et al., 2004; Forte et al., 2006). The physiologically based identification was consistent with the genotype prediction in the three animals (case MY88, case MY113, case MY123) where this had been carried out.

Single unit recording

Visually responsive units were recorded using parylene-coated tungsten microelectrodes (impedance 5–12 MΩ; F. Haere Co., Bowdoinham, ME, USA). The receptive field was centered on a stimulus monitor using a gimbaled, front-silvered mirror. Action potentials were amplified and their time of occurrence was measured under computer control with an accuracy of 100 μs. The amplitude and phase of the response were obtained by Fourier transformation of action potential discharge rate. The mean amplitude response (f0) was compared to the first harmonic (f1) amplitude and the larger of the two used as the responsiveness measure (Mechler & Ringach, 2002; Skottun et al., 1991). Cells were classified as belonging to the complex response class if the f0:f1 ratio was greater than unity and as simple class otherwise. This quantitative measure was consistent with receptive-field classifications made using hand-held stimuli.

Visual stimuli

Stimuli were drifting (4–5 Hz) square or sine wave gratings. Cone-selective gratings were generated by convolving the radiant energy spectra of the [R, G, B] gun-driven monitor phosphors with the predicted sensitivity spectra of marmoset cone mechanisms with peak sensitivity at 423 nm, 543 nm, 556 nm, and 563 nm (Tovée, Bowmaker, & Mollon, 1992; Travis, Bowmaker, & Mollon, 1988). The S-selective and ML-selective stimulus were set to achieve ~75% modulation of the relevant cone type with less than 4% modulation of the "silenced" cones (for details, see Forte et al., 2006). Gratings were generated using a VSG Series Three video signal generator (Cambridge Research Systems, Cambridge, UK) and presented on a cathode ray tube monitor (Reference Calibrator Plus, Barco, Kortrijk, Belgium) at a frame rate of 80 Hz and a mean luminance close to 25 cd/m^2. Stimuli were viewed through the natural pupil. Pupil diameter varied between ~2 and 4 mm, yielding retinal illuminance between 78 and 315 Td. The relatively small size of the marmoset eye (Troilo, Howland, & Judge, 1993) means that retinal flux will be about fourfold higher than for human at a given stimulus intensity. This makes it unlikely that rod photoreceptors contributed substantially to the responses recorded (Kremers, Weiss, Zrenner, & Maurer, 1997; but see also Yeh et al., 1995). Refraction was optimized at the beginning of each experiment by recording from the parvocellular layers of the dorsal lateral geniculate nucleus and using supplementary lenses to maximize single-unit responses to high spatial frequency achromatic gratings.

Optical imaging

Images were obtained through a cranial window above the representation of the fovea in V1 (based on visuotopic maps by Fritsches & Rosa, 1996), using established protocols [optical imaging system Imager3001 (Optical Imaging, Rehevot, Israel)]. The cortex was illuminated with 605-nm light. Reflected light was imaged using a 12-bit digital camera (40-Hz frame rate, pixel size 14 μm) focused 400–600 μm beneath the cortical surface. Image acquisition was synchronized to a constant phase of the respiratory cycle. Images were binned temporally to 500 ms/frame. For each image sequence, the initial 2.5 s was recorded while presenting a mean luminance gray screen, then the stimulus appeared for 4 s. A total of 7 to 17 s was recorded as required by the measurement. Stimuli were randomized and repeated 10–50 times for each stimulus set. Each stimulus set normally comprised varying values of the attribute that we wanted to map (for example, cone contrast), plus a blank. Focus level was normally set close to 400 μm below the cortical surface. Spatial frequency was normally set to 0.4 cycles per degree (CPD). Spatial modulation was normally square wave. Temporal frequency was normally set to 4 Hz. Stimulus field size was normally set to 20 degrees. Pilot analyses showed that these parameters reliably evoked strong intrinsic signals for both achromatic and cone-selective stimuli. For all comparisons shown in the following, only the stimulus dimension of interest was varied with other stimulus parameters held constant.

Image analysis

Single-condition images were prepared by calculating the change of reflectance from the blank condition and normalizing it to the blank level ($\Delta R/R$) for each pixel. Orientation maps were computed as follows.

1. For each time point in the frame sequence, the difference between the orientation single-condition image and the mean of all four orientations ("cocktail blank") was calculated.
2. The images obtained from 1 to 10 s following stimulus onset were averaged.
3. Images were filtered spatially (high pass: 700 × 700 μm boxcar, low pass: Gaussian, σ = 98 μm) to

remove pixel noise and large-scale differences between parts of the image.
4. The difference of each pixel from the mean of the image was calculated.

Thus, the resulting images show the orientation-dependent local change in response amplitude. Because only addition and subtraction of the single-condition images were applied, the resulting pixel values are in $\Delta R/R$ units allowing comparison across data sets.

Results

Primary afferents to the striate cortex (V1) come from all three main divisions (parvocellular, koniocellular and magnocellular) of the LGN, and the overall distribution of afferents is very well matched to the pattern of cytochrome oxidase reactivity (Ding & Casagrande, 1998; Lachica & Casagrande, 1992; Livingstone & Hubel, 1982; Roe et al., 2005; Wong-Riley, 1979; Yoshioka & Dow, 1996; Yoshioka, Blasdel, Levitt, & Lund, 1996). Figure 1 shows the pattern of afferent inputs to marmoset V1 as revealed by cytochrome oxidase histochemistry and shows schematically the relationship between the visual field representation and the target region for the optical imaging experiments. The central visual field (Figure 1A) is represented on the dorsolateral bank of the posterior occipital pole (Fritsches & Rosa, 1996; Roe et al., 2005; Schiessl & McLoughlin, 2003). A coronal section through this region (Figure 1B) shows the typical pattern of cytochrome oxidase reactivity reported for the primary visual cortex of diurnal primates (reviewed by Sincich & Horton, 2005). The dense continuous band of labeling in layer 4c (Figures 1B and 1C; nomenclature according to Brodmann) and a weaker continuous band in layer 6 are coincident with parvocellular and magnocellular afferents. By contrast, the inputs from koniocellular afferents comprise a continuous band in layer 4a (arrowheads, Figures 1B and 1C) and a patchy distribution to more superficial layers, where the axonal arbors of koniocellular afferents coincide with the cytochrome-oxidase-rich "blob" regions (Ding & Casagrande, 1998; Fitzpatrick et al., 1983; Hendry & Yoshioka, 1994; Lachica & Casagrande, 1992; Livingstone & Hubel, 1984; Solomon, 2002; Wong-Riley, 1979). The blob pattern (arrows in Figure 1B) is more readily appreciated in a tangential sections through V1 (arrows in Figure 1D).

The S-cone afferent signals to V1 most likely arise from the koniocellular pathway (Chatterjee & Callaway, 2003; Hendry & Reid, 2000; Martin et al., 1997; Szmajda et al., 2006), but the koniocellular pathway is likely to comprise several functional subdivisions, not all of which carry S-cone signals (Casagrande, 1994; Hendry & Reid, 2000; Solomon, White, & Martin, 1999; White, Solomon, & Martin, 2001; Xu et al., 2001). If (1) the S-cone axonal arbors are aligned with cytochrome-oxidase patches, and (2) the S-cone signal remains segregated in the post-afferent neurons, then the distribution of S-cone signal amplitude should be patchy. The main aim of our experiments is to discover whether this is the case.

We measured the functional input from S-cones to V1 neurons using two independent methods: single unit recordings and optical imaging of intrinsic signals. In the following section, we first describe responses of single units to drifting gratings presented in a variable-sized circular aperture. We next describe the optical imaging signal and examine the efficacy of S-cone contrast in evoking intrinsic signals. Finally, we compare the amplitude of the intrinsic signal to the single unit results under different chromatic conditions.

S-cone input to V1 neurons

The blue-on and blue-off cells in the retina and LGN receive dominant functional input from S-cones, whereas other cell classes receive less input from S-cones than would be expected on the basis of random connections (Derrington, Krauskopf, & Lennie, 1984; Lee, Valberg, Tigwell, & Tryti, 1987; Sun et al., 2006; Szmajda et al., 2006; but see also Chatterjee & Callaway, 2002). If this functional segregation is preserved in V1, one would expect to find some cells dominated by S-cone inputs, but only weak S-cone inputs to other cells. In order to test this, we recorded the responses of V1 neurons to S-cone-selective and achromatic drifting gratings. The gratings were presented in apertures of variable diameter. By finding the aperture yielding maximal response rate, we thus obtained a measure of S-cone input under conditions optimized to the classical receptive field. Responses were also measured for larger stimuli, which approximate closely the stimulus conditions used for measuring optical signals.

Figures 2A and 2B illustrate responses of a typical V1 simple cell to achromatic sinusoidally modulated gratings. This is a typical V1 neuron showing band-pass spatial frequency tuning (Figure 2A) and strong orientation selectivity (Figure 2B). Figure 2C shows the response of the same cell to achromatic sine gratings of optimal spatial frequency and orientation presented in variable diameter apertures. The cell shows spatial summation below the optimum aperture diameter close to 3 deg. The response declines for larger apertures, presumably due to suppression from the "silent" extra-classical surround of the receptive field (Bardy, Huang, Wang, FitzGibbon, & Dreher, 2006; DeAngelis, Freeman, & Ohzawa, 1994; Sceniak, Ringach, Hawken, & Shapley, 1999; Solomon & Lennie, 2005). This behavior is well described by a difference-of-Gaussians model (DeAngelis et al., 1994; Sceniak et al., 1999). Response of this cell to S-cone-selective gratings (Figure 2C) never exceeds 10.1% of the response amplitude to achromatic gratings. In this figure

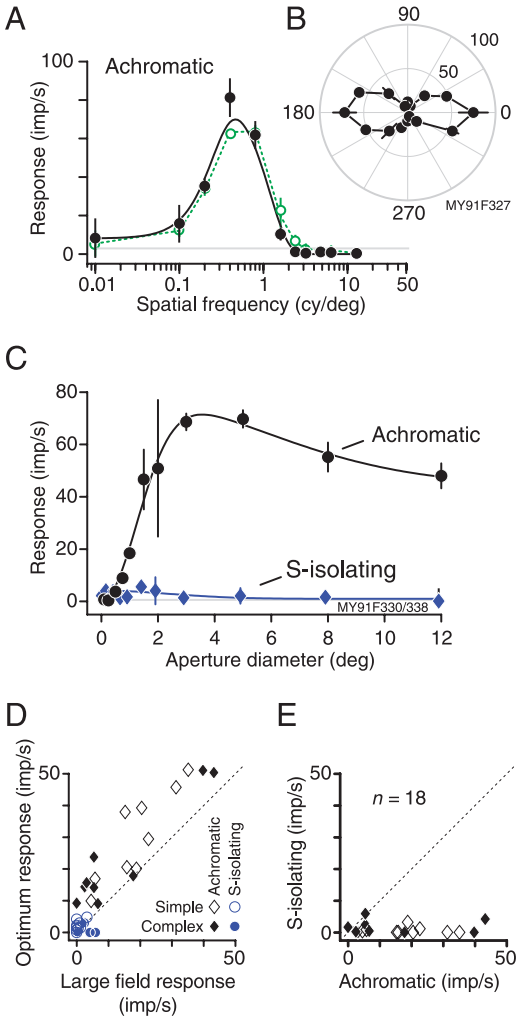

Figure 2. Responses of V1 cortical neurons to achromatic or S-cone-specific modulation in male marmosets. (A) Spatial frequency, (B) direction, and (C) aperture responses of a V1 simple cell obtained with (ACH) achromatic (SWS) or S-cone-selective sine gratings. Solid black symbols indicate the first harmonic (f1) response. Error bars show standard deviations. For some measurements the error bars are smaller than the symbols. Solid black curves show the best fit difference-of-Gaussians; horizontal lines indicate f1 response to zero contrast. Dashed green line and open symbols show the mean discharge rate (f0) in panel A. The f0 response amplitude is similar to f1 response amplitude, as expected for simple class cells. The angle in the polar plot (B) shows the drift direction of the stimulus grating, radius shows response amplitude. Temporal frequency 4 Hz, spatial frequency in panels B and C: 0.4 cycles/deg. (D–E) Comparison of responses of a sample of V1 cells (n = 18) to achromatic and S-cone-selective gratings. Amplitudes are normalized for stimuli of unit contrast. (D) Responses to large (12 deg) *vs.* optimum sized apertures. Black symbols, responses to achromatic stimuli; blue symbols, responses to S-cone-selective stimuli; open symbols, simple cells; closed symbols, complex cells. (E) Comparison of responses to achromatic and S-cone-selective gratings presented in large (12 deg) apertures.

the response amplitudes have been normalized for stimuli of unit contrast, that is, amplitudes are divided by the cone contrast (0.7–0.75) for S-cone-selective gratings. Thus, even when the lower cone contrast of the S-cone-selective grating is taken into account, the response to S-cone modulation is negligible.

Similar measurements made in other V1 cells (n = 18) with receptive fields within five degrees of the fovea yielded very similar results. For each V1 cell the aperture tuning curves were measured at the optimal orientation and spatial frequency (e.g., Figures 2A and 2B). In nearly all cells the magnitude of responses was reduced when large-field achromatic gratings were used (Figure 2D), and there was no aperture size at which S-cone-selective gratings evoked large responses (Figures 2D and 2E). No significant difference in response amplitude was seen between simple (open symbols) and complex (closed symbols) cells (p = 0.96, Wilcoxon rank-sum test), and the amplitude ratio of S-cone to achromatic responses for 12 deg apertures was always low (mean ratio 0.047, *SD* 0.088). These data are consistent with our more extensive analysis of S-cone inputs to V1 cells in marmosets (Hashemi-Nezhad et al., 2008). In that study, we reported relative S-cone weights to V1 cells measured using optimally sized apertures and found average 8% functional input from S-cones (*SD* 6.0, n = 49; Hashemi-Nezhad et al., 2008). Furthermore, in that study we found no significant difference in S-cone weight when responses of cells located in the supragranular and granular layers (1–4) were compared to the responses of cells located in the infragranular layers 5 and 6 (mean S-cone weight for layers 1–4: 9.8%, *SD* 5.9%, n = 22; layers 5 and 6: 6.6%, *SD* 6.6%, n = 15, p = 0.07, Wilcoxon rank-sum test; Hashemi-Nezhad et al., 2008). Several studies in the cortex of macaque monkeys have also found only weak S-cone inputs to the majority of V1 neurons (Conway & Livingstone, 2006; Horwitz et al., 2005; Johnson et al., 2004; Solomon & Lennie, 2005). However, we cannot rule out the possibility that there does exist a small subset of V1 cells with strong S-cone input (Conway & Livingstone, 2006; Horwitz et al., 2005; Johnson et al., 2004; Solomon & Lennie, 2005) which we simply did not encounter.

Time course of the optical response

We performed imaging of visually evoked intrinsic optical responses from the primary visual cortex of four marmosets. We used illumination at a wavelength of 605 nm to reveal the activity-dependent changes in oxygen saturation of hemoglobin (Grinvald, Lieke, Frostig, Gilbert, & Wiesel, 1986). This signal is an indirect correlate of the neural response: the hemodynamic state of the brain changes constantly and many changes are not directly related to local neuronal activity (Berwick et al., 2005; Mayhew et al., 1996; Vanzetta, Hildesheim, &

Grinvald, 2005). Therefore, before measuring presumed S-cone driven activity, we tested whether visual stimuli evoke an optical signal that is consistent with the expected neuronal response.

We first determined the time course of the optical response. Figure 3A shows the area sampled for one such measurement (4.4 × 9.8 mm) superimposed on the surface of the cortex. The imaged field typically included superficial dural blood vessels (an example runs from bottom center to middle right of the imaged field in Figure 3A), but these vessels did not show any stimulus-related change in signal and therefore do not appear in the averaged single-condition maps. Figure 3B shows the mean fractional change of reflectance across image pixels ($\Delta R/R$, see Methods) following presentation of an achromatic grating. Focal level was close to 400 μm below the cortical surface. The zero value on the ordinate axis indicates no change relative to the (separately recorded) blank condition. A reflectance decrease is evident within the first 500 ms after stimulus onset, with maximum change reached at close to 6.5 s. This time course is consistent with a reduced oxygen-saturation of hemoglobin caused by metabolic activity of neurons and is characteristic of the first phase of the intrinsic optical signal (often called "initial dip"). Hereinafter we refer to this phase of the signal as the optical response. The response amplitudes (dynamic range $\Delta R/R$ ~5–8 × 10^{-3} [0.5%-0.8%]) compare favorably to other studies of intrinsic optical signal in marmoset cortex (McLoughlin & Schiessl, 2006; Roe et al., 2005; Schiessl & McLoughlin, 2003). The signal time course is somewhat slower than those reported elsewhere for visual and somatosensory

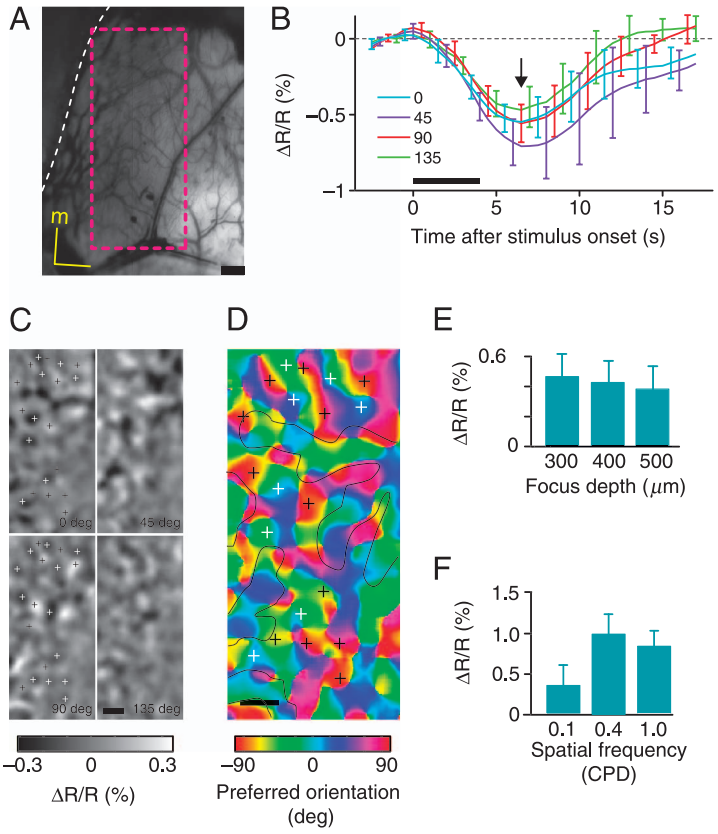

Figure 3. Optical imaging of visual responses in marmoset V1. (A) The cortical region imaged under green light illumination showing blood vessels of the surface (case MY123). Dashed magenta line shows the area analyzed. Dashed white line indicates the border of the craniotomy. (B) Time course of the normalized change of reflectance on presentation of achromatic drifting gratings at four different orientations. Data points here and in following time course plots show averages and standard deviations. Stimuli were presented for 4 s as marked by the black bar on the time axis. The reflectance change reached its maximum at 6.5 s (arrow) after stimulus onset. (C) Gray scale maps representing the differential signal to gratings of four orientations relative to the mean of all orientations, after spatial filtering as described in the text. Images were taken 6.5 s after stimulus onset. (D) Orientation angle map showing the preferred orientation of the optical response. The black contours show the boundaries of the analyzed regions. Small cross markers indicate points of high orientation selectivity; a complementary pattern of activity in response to orthogonal stimulus orientations can be seen by reference to these marks in part C. (E) Average signal intensity at different focal depths below the cortical surface for 0.1 cycle per degree (CPD) achromatic gratings (case MY113). (F) Average signal intensity for low (0.1 CPD, case MY113), intermediate (0.4, CPD, case MY120), and high (1 CPD, case MY120) spatial frequency achromatic gratings. Scale bars = 1 mm in panels A, C, D. Error bars in E, F show standard deviations.

cortices (Chen-Bee, Agoncillo, Xiong, & Frostig, 2007; Lu & Roe, 2007; Malonek et al., 1997) but is similar to the signal time course reported by Meister and Bonhoeffer (2001) for rat olfactory bulb. In the present study, signals of comparable amplitude and time course were obtained in all four marmosets.

Orientation map in marmoset V1

As indicated in Figure 3B, the average signal amplitude for achromatic stimuli was similar across grating orientation, representing on average ~0.5–0.8% reflectance change. For any given pixel, however, the response amplitude depended on the orientation of the grating. Reflectance maps (calculated as described in the Methods section) for 4 stimulus orientations are shown Figure 3C. Darker pixels correspond to more active cortical regions. These maps closely resemble the pattern of orientation preference columns previously described in marmoset V1 (McLoughlin & Schiessl, 2006; Roe et al., 2005). The orientation preference of each location can be obtained by pixel-by-pixel vectorial summation of the orientation single-condition maps of Figure 3C. The map of resultant preferred orientations is shown color-coded in Figure 3D. In regions containing major blood vessels that supply extended regions of the cortex, the hemodynamic signal measured by optical imaging becomes poorly correlated with the activity in the underlying gray matter (Berwick et al., 2005; Vanzetta et al., 2005). We excluded such regions (marked by black contours in Figure 3D) from further analysis and the term "region of interest" (ROI) is used hereinafter to refer to the non-excluded regions in the field of view. In all cases the time course and spatial pattern of optical responses obtained was consistent with stimulus-dependent activation in the imaged region.

Orientation maps of comparable quality were obtained for one other animal (case MY113). For two other animals (cases MY121 and MY123), the orientation map was however much weaker, despite the fact that robust average reflectance changes could be measured. We could find no obvious correlation of orientation map strength with the physiological state of the preparation or responsiveness of single units recorded in V1 or the LGN in these experiments. The implications of this variability are discussed further below.

In one animal (case MY121) we tested the effect of imaging focus level on the strength of the intrinsic signal. Figure 3E shows a mild decrease in signal intensity with increasing focal depth, as expected from the decreasing visibility of blood vessels that are the main source of the intrinsic signal. Figure 3F shows that, consistent with spatial band-pass properties of the majority of neurons in marmoset V1 (Forte, Hashemi-Nezhad, Dobbie, Dreher, & Martin, 2005), the signal for 0.4 CPD gratings is stronger than the signal for 0.1 CPD or 1.0 CPD gratings. We therefore made the great majority of measurements at 0.4 CPD.

Optical response to cone-selective and achromatic stimuli

Figure 4 shows the time course and contrast dependence of intrinsic optical signals in response to achromatic and cone-selective stimuli. The maximum stimulus-evoked changes measured by optical imaging are in the order of 1% of the baseline signal, which together with noise from the on-going hemodynamic fluctuations of the cortex make it difficult to detect small responses. We therefore measured the statistical significance of responses as a function of the time after stimulus onset. For each pixel, we performed a *t*-test with the null hypothesis that $\Delta R/R$ is zero (no change relative to the blank condition) and a confidence level of 95%. The sample comprised 10 consecutive experimental "blocks" × 2 orientations to give a total of 20 measurements *per* pixel for each contrast. Each block is averaged from five stimulus presentations; each image is an average of 20 camera frames; and each pixel averages light over a larger region due to light scatter. Thus, we are testing the variance of the signal that remains after all this spatio-temporal averaging.

Figure 4A shows the emergence of responses to 75% achromatic contrast. Red pixels show *p*-values above the criterion of 0.05. Gray pixels show log-transformed probability for significantly activated pixels. Prior to stimulus onset (time points ≤0 s), spontaneous fluctuations result in occasional pixels crossing the criterion. Following stimulus onset (indicated by the arrow in Figure 4A), the number of pixels with significant signal increases rapidly and extends throughout the region of interest within two seconds. The cortex remains significantly activated throughout the "initial dip" phase. Figures 4B and 4C show the emergence of significant responses for ML- and S-cone-selective stimuli, in the same format as Figure 4A. All three conditions are matched for cone contrast (70%). Two features are immediately obvious. First, the cone-selective stimuli, like the achromatic stimulus, produce significant activation of all pixels in the region of interest. Second, there is an almost identical pattern of cortical activation in the three response conditions, suggesting there is no specific segregation of S- and ML-cone signals across the cortical surface.

All pixels crossed the criterion level ($p < 0.05$) within three seconds of stimulus onset for both cone-selective conditions. Similar results were obtained for the other three cases studied. For the S-cone-selective condition, 100% of pixels reached $p < 0.05$ by 4.5 s for case MY120. Cases MY113 and MY121 yielded weaker signals; the S-cone-selective signal (at $p < 0.05$) in these cases was reached by respectively 75% and 80% of pixels within six seconds of stimulus onset. No clear sign of spatial

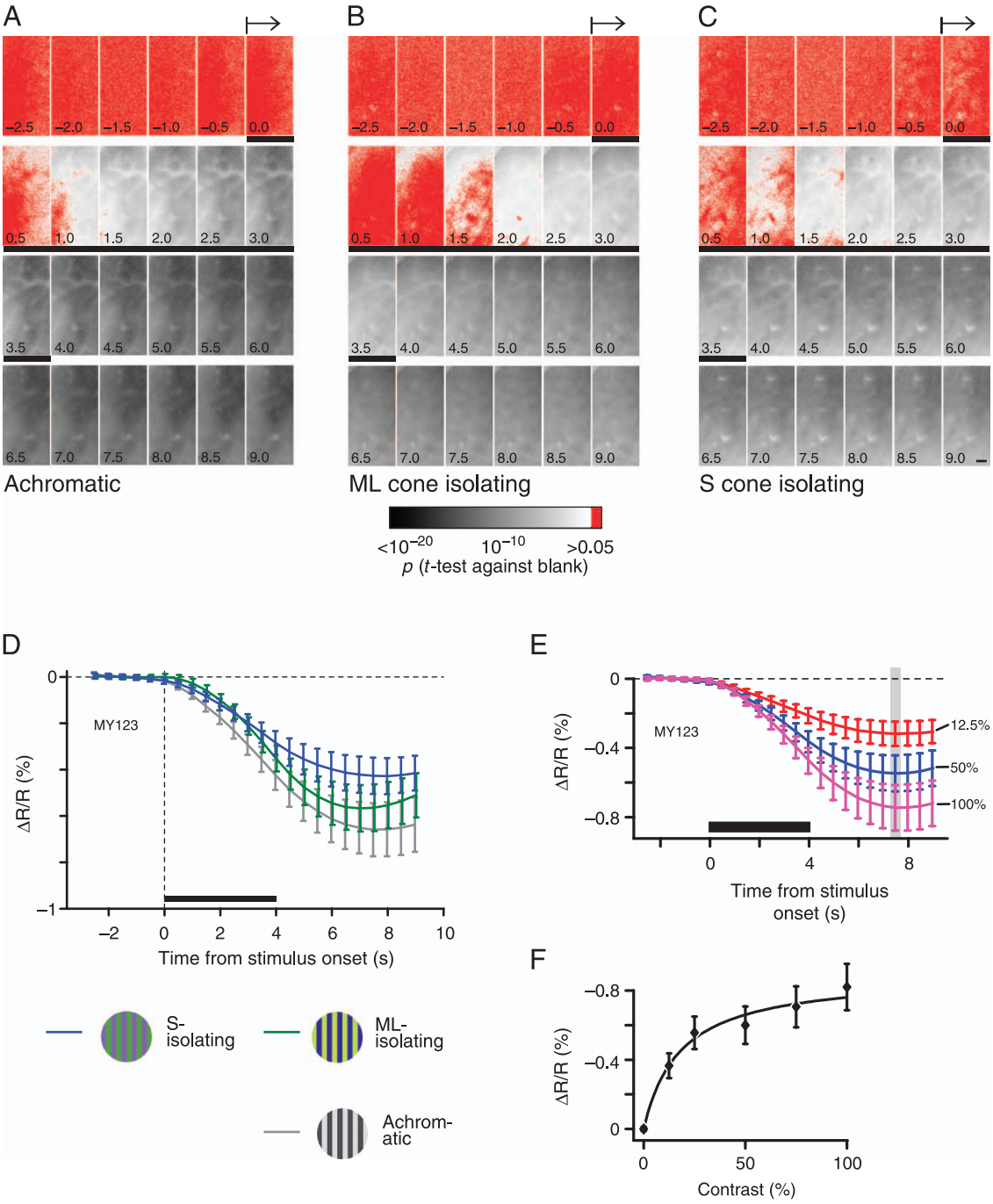

Figure 4. Cortical activation by achromatic and cone-selective stimuli. (A–C) Frame sequences showing the emergence of significant activation during presentation of (A) achromatic, (B) ML-cone-selective, and (C) S-cone-selective gratings (case MY123). All pixels showed statistically significant activity ($p < 0.05$) within three seconds of stimulus onset. Time (s) relative to the beginning of the stimulus is indicated in each frame. The duration of the stimulus is indicated by the black bars under the images. The color of image pixels (color scale at the bottom) indicates the *p*-values from *t*-tests comparing activity for stimulated and blank conditions for each pixel. (D) Time courses of the optical responses. All three responses follow similar time courses but responses to cone-selective stimuli are smaller in amplitude. Grating patches show the approximate appearance of the three stimuli. (E) Optical signal time courses on presentation of achromatic drifting gratings at various contrasts. The stimuli were presented for 4 s as indicated by black bars on the time axes. The reflectance change reached its maximum at 7.5 s (gray bar) after stimulus onset. (F) Contrast response function of the imaged regions at 7.5 s following stimulus onset. Data points show mean and standard deviation of pixels calculated from the peak responses in panel E. Some saturation is evident at high contrast. Solid lines show best fit Naka–Rushton curves. Scale bar (1 mm) in the lower right frame of panel C applies to panels A, B, C.

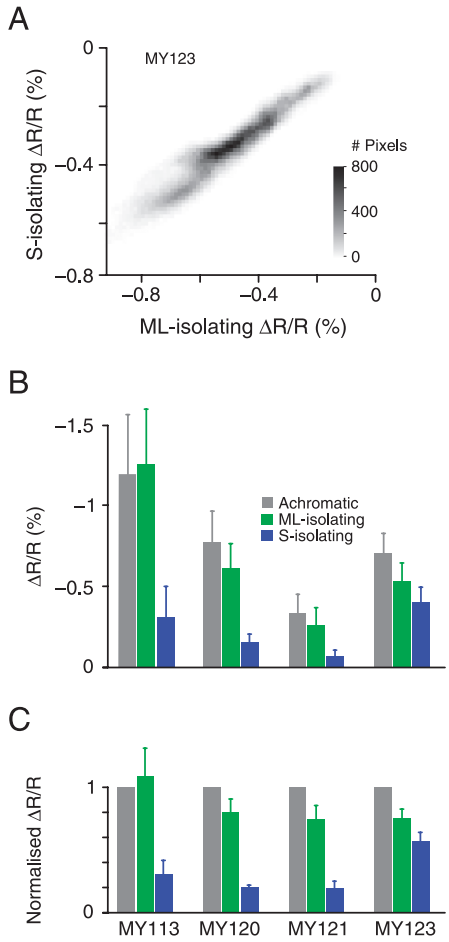

Figure 5. (A) Scatterplot showing pixel distributions of peak response amplitude for ML-cone-selective and S-cone-selective stimuli. Note the strong positive correlation. (B) Peak amplitude of optical responses in V1 to different chromatic conditions. Optical signal amplitudes are greater for ML-cone-selective gratings than for S-cone-selective gratings at equal cone contrast. (C) Responses from (A) normalized in each pixel to the achromatic response.

variation in response intensity was seen in any of the four cases analyzed. We demonstrate below that this qualitative impression is confirmed by a pixel-by-pixel cross correlation between the different chromatic conditions.

Figure 4D shows response amplitude and time course for the stimuli shown in Figures 4A–4C. Each curve shows averages of four orientations and all pixels of the region of interest. Both cone-selective stimuli evoked optical responses similar in time course to those obtained with achromatic stimuli. That the signal time course for achromatic stimuli is largely independent of contrast is shown in Figure 4E. Response amplitude at 7.5 s after stimulus onset is plotted against contrast in Figure 4F. The solid line (Figure 4F) shows the contrast–response relationship is well approximated ($r^2 > 0.95$) by a hyperbolic ratio model function with an exponent of 1 (Albrecht & Hamilton, 1982; Naka & Rushton, 1966). The model fits yielded half saturation contrast C_{50} = 17.9% and 33.1%; maximum response $R_{max} = -8.96 \times 10^{-3}$ and -0.19×10^{-3} for cases MY123 and MY121, respectively. Similar values for the half-saturation contrast were obtained when we fit contrast–response functions individually for each pixel (C_{50} = 19.2 ± 2.0 and 45.7 ± 15.0). At first sight these data are not consistent with linear contrast sensitivity reported for intrinsic signals in macaque V1 (Lu & Roe, 2007), but it should be noted that over the signal range which these authors report ($\Delta R/R$ less than 0.2%), the signals we measured were also approximately linear with contrast. Even at the lowest contrast tested (12.5%) a statistically significant response appeared in all pixels within three seconds of stimulus onset. We conclude that the achromatic contrast threshold for signal detection with optical imaging is below 12.5%.

Comparison of response amplitude

The thalamic S-cone afferents to visual cortex are S/ML-cone opponent and normally respond more vigorously to S-cone than to achromatic modulation (Chatterjee & Callaway, 2003; Derrington et al., 1984; Hashemi-Nezhad et al., 2008; Szmajda et al., 2006). If the afferents are patchily distributed, then the ratio of S-cone to achromatic response amplitude would be expected to show even stronger spatial variation than the S-selective minus baseline condition. However, we found that S and ML activation is positively correlated. This result is summarized in Figure 5. Figure 5A shows the distribution of pixel values for S-selective and ML-selective conditions in case MY123. This shows that points in the image that are strongly activated by the S-cone-selective grating are also strongly activated by the ML-cone-selective grating. A comparison of the four animals studied is shown in Figures 5B and 5C and Table 1. In Figure 5C, response

	Response amplitude ($\Delta R/R \times 10^{-3}$)			Cone contrast		
Case	Achromatic	ML selective	S selective	Achromatic	ML selective	S selective
MY113	−11.68	−12.27	−3.49	1.00	0.70	0.77
MY120	−7.72	−6.10	−1.58	1.00	0.70	0.70
MY121	−3.38	−2.60	−0.70	0.75	0.75	0.75
MY123	−7.06	−5.33	−4.04	0.70	0.70	0.70

Table 1. Response amplitude and cone contrasts.

amplitude for the cone-selective conditions is normalized to the achromatic response magnitude on a pixel-by-pixel basis. For the two animals in which achromatic and cone-selective contrasts were matched (cases MY121 and MY123), the relationship (ACH > ML > S) is consistent for essentially all of the regions analyzed (MY121, 100%; MY123, 99.9% of pixels). Furthermore, in these cases response amplitude for the ML-cone-selective condition is always lower than response amplitude for the achromatic condition (Figure 5B). Since the achromatic gratings had the same cone contrast and other parameters as ML-selective ones, the additional signal in the achromatic condition can thus be ascribed to functional input from S-cones.

A consistent pattern is seen in the other two animals (cases MY113 and MY120), where contrast for the achromatic stimulus was higher than that for the cone-selective conditions. Overall, no pixels in the imaged regions of cortex for any animal studied responded preferentially to S-cone-selective over ML-cone-selective stimulation.

As shown in Figure 4F, even the lower values of achromatic contrast we used (70–75%) are likely to be on the saturating part of the contrast response function. If S-cone inputs converged additively with ML-inputs before the saturation stage, one would expect the achromatic response to be less than the sum of cone-selective responses. Such response compression could explain the relationship of the three responses in cases MY113 and MY123. In the two other cases, the ML- and S-cone responses add almost perfectly to give the achromatic amplitude [(ML + S) / ACH = 1.00 and 0.94, for MY120 and MY121 respectively; Figure 5C].

Overall, our results suggest that the response to achromatic contrast is an additive combination of responses to S-cone and ML-cone-selective stimuli. This argument is however limited by the fact that a substantial contribution to optical signals may arise from subthreshold neuronal activity (Viswanathan & Freeman, 2007).

Discussion

Our main result is not consistent with the hypothesis that koniocellular S-cone afferents cause selective activation in cytochrome-oxidase-rich ("blob") regions in the superficial layers of V1. Rather, our imaging and single-unit recordings support the conclusion that activity arising from S-cones provides only weak or subthreshold activation for the majority of V1 neurons in marmosets. Here we consider first the relation of our results to previous intrinsic signal imaging studies then consider the relation of our results to single-cell and anatomical studies of color processing in the primate cerebral cortex.

Relation to previous imaging studies

To our knowledge, this is the first intrinsic signal imaging study to specifically measure the effect of contrast-matched cone-selective gratings. This enabled us to assess directly the effect of cone contrast on cortical activation, using a non-differential (signal minus baseline) comparison. We found no evidence for spatial variation in cortical activation by cone-selective gratings, despite the fact that these stimuli produced significant, contrast-dependent cortical activation. Previous studies in macaques and marmosets used chromatic (red-green and blue-yellow) gratings and report mostly differential comparison with luminance-varying gratings to infer the distribution of color signals (Landisman & Ts'o, 2002a, 2002b; Lu and Roe, 2008; Roe et al., 2005). Consistent with our results, there is consensus from these studies that non-differential signals reveal only weak anisotropies in distribution of responses to chromatic gratings. Xiao et al. (2007) reported non-differential optical signals from macaque V1, in response to spatially uniform color change. They report a hue-selective signal with spatial distribution consistent with blob domain density. The dynamic signal range they report ($\Delta R/R \sim 7 \times 10^{-4}$) is weaker than the dynamic range of signals we measured in the current study ($\sim 5 \times 10^{-3}$), which makes it unlikely that in our experiments a strong S-cone map is present but we failed to detect it. Because the colored stimuli used by these authors do not produce uniform excitation or adaptation conditions for the different cone mechanisms, their results cannot be easily related to cone signal distribution in the cortex. In our experiments we delivered greater cone-selective contrast than those that has been achieved in previous studies, which means that any spatially clustered signal from the cortex should be stronger than that revealed by previous studies. However, we did not see any selective signal. In summary, our negative result is broadly consistent with the picture emerging from imaging and single-unit studies of cortex in trichromatic macaques: If there is tangential segregation of S-cone signals in V1, then it is weaker than the segregation which gives rise to other functional maps such as retinotopy, orientation, and ocular dominance.

For reasons that remain unclear, we found high variability between marmosets in the overall strength of the orientation map. We saw significant cortical activation by achromatic, S- and ML-cone-selective stimuli in cases with both weak and strong orientation maps, suggesting that the physiological state of the cortex *per se* had not been compromised. Although there is agreement that adult marmosets show only weak and variable ocular dominance maps (Markstahler, Bach, & Spatz, 1998; McLoughlin & Schiessl, 2006; Roe et al., 2005; Sengpiel, Troilo, Kind, Graham, & Blakemore, 1996; Spatz, 1989), previous studies consistently showed robust orientation maps in marmoset V1 (McLoughlin & Schiessl, 2006; Roe et al., 2005; Schiessl & McLoughlin, 2003).

We cannot rule out the possibility that a factor such as anesthetic state of the animals has reduced our ability to measure any spatial signal in the marmoset cortex (Greenberg, Houweling, & Kerr, 2008). In the present study, to maintain general anesthesia, we used sufentanil citrate whereas sodium pentothal was used in several previous imaging studies on marmoset cortex (McLoughlin & Schiessl, 2006; Roe et al., 2005; Sengpiel et al., 1996). However, Roe and colleagues (2005) used both agents (in different animals) and did not report individual differences in the strength of orientation maps. Their results thus suggest that anesthetic regime is unlikely to be a critical factor. Furthermore, under the same experimental conditions as the optical imaging experiments, we consistently measured robust single-unit responses in V1 (Figure 2). Finally, again under the same experimental regime used for the imaging experiments, neurons dominated by S-cone inputs ("blue-on" and "blue-off" cells) are readily recorded in the LGN (Szmajda et al., 2006; Victor, Blessing, Forte, Buzás, & Martin, 2007). All these observations are consistent with our conclusion that signals arising in S-cone afferents are not spatially compartmentalized in V1 in anesthetized marmosets.

Relation to previous single-cell and anatomical studies

Blasdel and Lund (1983) reconstructed two blue-on afferents in macaque cortex; one ramified in layer 4Cβ and the other showed very fine and diffuse terminals in layer 1 and layer 6. In an electrophysiological survey, Chatterjee and Callaway (2003) found that in macaques afferent S-cone signals are segregated to the lower border of layers 3B and 4A. This raises the possibility that the S-cone afferents terminate selectively on a subgroup of color-selective cells within these layers. Indeed, Cottaris and De Valois (1998) found that cells with sluggish S-cone input in macaques were segregated to the supragranular layers, but Johnson et al. (2004) found cells with strong S-cone input (10/247) were mostly located in infragranular layers. Other studies do not report strong laminar segregation of cells with strong S-cone input (Horwitz et al., 2005; Solomon & Lennie, 2005). A definitive answer would require an extensive targeted sample of single cells from layers 3B and 4A, with the specific goal of measuring the functional weight of S-cone input. In the present study, we did not see an obvious change in signal strength as a function of focus depth within the cortex (Figure 3E) but fine-grained analysis might yet reveal that optical responses to S-cone signals do show laminar segregation.

There is clear agreement in results from all primate species so far that direct innervation of blob regions in the supragranular layers arises from the koniocellular pathway (Casagrande et al., 2007; Ding & Casagrande, 1997; Fitzpatrick et al., 1983; Hendry & Yoshioka, 1994; Lachica & Casagrande, 1992; Livingstone & Hubel, 1982; Solomon, 2002). Given our previous evidence that cells receiving strong S-cone input (blue-on and blue-off cells) are segregated to the koniocellular pathway (Martin et al., 1997; Szmajda et al., 2006), we were at first surprised to find no spatial segregation of S-cone signals in the present experiments. For example (cf. Figure 1), we know that blob density in marmoset V1 is ~4–5 blobs/mm^2 (Roe et al., 2005; Solomon, 2002; Spatz, Illing, & Vogt-Weisenhorn, 1994), so the field of view in Figure 4 (~4 × 8 mm) would be expected to include over 100 blobs. Our results using cone-selective stimuli are nevertheless consistent with Roe et al.'s (2005) result showing that there is no spatial signal for isoluminant chromatic (blue-yellow) gratings and extend these findings by showing that responses to cone-selective stimuli cause significant contrast-dependent increases in cortical activity (Figure 4). Chatterjee and Callaway (2003) showed that off-type S-cone afferents are distributed in patchy fashion whereas on-type afferents were more consistently encountered in layers 3B and 4A, suggesting more uniform coverage of these cortical layers. This raises the possibility that S-cone afferents do not target specifically the blob regions in layer 3B but rather project more diffusely to the continuous cytochrome oxidase-rich band in layer 4A (Figure 1). This possibility would be consistent with the (circumstantial) evidence that nocturnal primate species lacking functional S-cones (the prosimian bush baby *Galago senegalensis* and owl monkey *Aotus trivirgatus*) nevertheless show a very similar pattern of koniocellular inputs to the blobs as do (S-cone expressing) marmosets, macaques, and squirrel monkeys (Casagrande et al., 2007; Ding & Casagrande, 1998; Fitzpatrick et al., 1983; Horton & Hubel, 1981; Lachica & Casagrande, 1992; Livingstone & Hubel, 1982; Solomon, 2002; Xu et al., 2004). Indeed, as pointed out elsewhere, in species that lack S-cones, the cytochrome oxidase blobs cannot (*ipso facto*) process S-cone signals (Casagrande & Xu, 2003). The fact that *Galago* and *Aotus* also lack thalamocortical inputs to layer 4A (Diamond, Conley, Itoh, & Fitzpatrick, 1985) could thus be interpreted as absence of S-cone afferents to this cortical layer.

Although there is now general agreement that the segregation of color-selective cells to blob regions is not as strict as that envisioned more than twenty years ago by Livingstone and Hubel's (1984), the controversy is not fully resolved (reviewed by Sincich & Horton, 2005). Although we see no evidence for a specific S-cone color map, we cannot rule out the possibility that the suppressive effect of large-field grating stimuli (Figure 2) has masked a weak but specific input from S-cone-carrying afferents to blob regions. If the functional image is dominated by subthreshold activity (Viswanathan & Freeman, 2007), perhaps even arising in other parts of the cortex, then S-cone signals could be specifically processed by a rare population of color-selective cells even outside V1 and hence distributed widely through the

cortical network to yield the signals we measured. Different kinds of experiments are required to address specifically these hypotheses.

Acknowledgments

We thank U Grünert, J Levitt, A Roe, and C Tailby for helpful comments, D. Matin, P. Jusuf, and B. Eriköz for the histological analysis, A. Lara for technical assistance, and A. Metha for valuable programming assistance. This study was supported by the Australian National Health and Medical Research Council Grant 253621, the Australian Research Council Grant 451481, and the Victorian Lions Foundation. Author BAS was supported by a University of Melbourne graduate study scholarship.

Commercial relationships: none.
Corresponding author: Paul R. Martin.
Email: prmartin@unimelb.edu.au.
Address: National Vision Research Institute of Australia, Cnr Cardigan & Keppel Sts, Carlton, Victoria 3053, Australia.

References

Albrecht, D. G., & Hamilton, D. B. (1982). Striate cortex of monkey and cat: Contrast response function. *Journal of Neurophysiology, 48,* 217–237. [PubMed]

Bardy, C., Huang, J. Y., Wang, C., FitzGibbon, T., & Dreher, B. (2006). 'Simplification' of responses of complex cells in cat striate cortex: Suppressive surrounds and 'feedback' inactivation. *The Journal of Physiology, 574,* 731–750. [PubMed] [Article]

Berwick, J., Johnston, D., Jones, M., Martindale, J., Redgrave, P., McLoughlin, N., et al. (2005). Neurovascular coupling investigated with two-dimensional optical imaging spectroscopy in rat whisker barrel cortex. *European Journal of Neuroscience, 22,* 1655–1666. [PubMed]

Blasdel, G. G., & Lund, J. S. (1983). Termination of afferent axons in macaque striate cortex. *Journal of Neuroscience, 3,* 1389–1413. [PubMed] [Article]

Blessing, E. M., Solomon, S. G., Hashemi-Nezhad, M., Morris, B. J., & Martin, P. R. (2004). Chromatic and spatial properties of parvocellular cells in the lateral geniculate nucleus of the marmoset (*Callithrix jacchus*). *The Journal of Physiology, 557,* 229–245. [PubMed] [Article]

Casagrande, V. A., Yazar, F., Jones, K. D., & Ding, Y. (2007). The morphology of the koniocellular axon pathway in the macaque monkey. *Cerebral Cortex, 17,* 2334–2345. [PubMed]

Casagrande, V. A. (1994). A third parallel visual pathway to primate area V1. *Trends in Neurosciences, 17,* 305–310. [PubMed]

Casagrande, V. A., & Xu, X. (2003). Parallel visual pathways: A comparative perspective. In L. M. Chalupa, & J. S. Werner (Eds.), *The visual neurosciences* (pp. 494–506). Cambridge, MA: The MIT press.

Chatterjee, S., & Callaway, E. M. (2002). S cone contributions to the magnocellular visual pathway in macaque monkey. *Neuron, 35,* 1135–1146. [PubMed] [Article]

Chatterjee, S., & Callaway, E. M. (2003). Parallel colour-opponent pathways to primary visual cortex. *Nature, 426,* 668–671. [PubMed]

Chen-Bee, C. H., Agoncillo, T., Xiong, Y., & Frostig, R. D. (2007). The triphasic intrinsic signal: Implications for functional imaging. *Journal of Neuroscience, 27,* 4572–4586. [PubMed] [Article]

Conway, B. R., & Livingstone, M. S. (2006). Spatial and temporal properties of cone signals in alert macaque primary visual cortex. *Journal of Neuroscience, 26,* 10826–10846. [PubMed] [Article]

Cottaris, N. P., & De Valois, R. L. (1998). Temporal dynamics of chromatic tuning in macaque primary visual cortex. *Nature, 395,* 896–900. [PubMed]

DeAngelis, G. C., Freeman, R. D., & Ohzawa, I. (1994). Length and width tuning of neurons in the cat's primary visual cortex. *Journal of Neurophysiology, 71,* 347–374. [PubMed]

Derrington, A. M., Krauskopf, J., & Lennie, P. (1984). Chromatic mechanisms in lateral geniculate nucleus of macaque. *The Journal of Physiology, 357,* 241–265. [PubMed] [Article]

Diamond, I. T., Conley, M., Itoh, K., & Fitzpatrick, D. (1985). Laminar organization of geniculocortical projections in *Galago senegalensis* and *Aotus trivirgatus*. *Journal of Comparative Neurology, 242,* 584–610. [PubMed]

Ding, Y., & Casagrande, V. A. (1997). The distribution and morphology of LGN K pathway axons within the layers and CO blobs of owl monkey V1. *Visual Neuroscience, 14,* 691–704. [PubMed]

Ding, Y., & Casagrande, V. A. (1998). Synaptic and neurochemical characterization of parallel pathways to the cytochrome oxidase blobs of primate visual cortex. *Journal of Comparative Neurology, 391,* 429–443. [PubMed]

Fitzpatrick, D., Itoh, K., & Diamond, I. T. (1983). The laminar organization of the lateral geniculate body and the striate cortex in the squirrel monkey (*Saimiri sciureus*). *Journal of Neuroscience, 3,* 673–702. [PubMed] [Article]

Forte, J. D., Blessing, E. M., Buzás, P., & Martin, P. R. (2006). Contribution of chromatic aberrations to color signals in the primate visual system. *Journal of Vision, 6*(2):1, 97–105, http://journalofvision.org/6/2/1/, doi:10.1167/6.2.1. [PubMed] [Article]

Forte, J. D., Hashemi-Nezhad, M., Dobbie, W. J., Dreher, B., & Martin, P. R. (2005). Spatial coding and response redundancy in parallel visual pathways of the marmoset *Callithrix jacchus*. *Visual Neuroscience, 22,* 479–491. [PubMed]

Fritsches, K. A., & Rosa, M. G. (1996). Visuotopic organisation of striate cortex in the marmoset monkey (*Callithrix jacchus*). *Journal of Comparative Neurology, 372,* 264–282. [PubMed]

Greenberg, D. S., Houweling, A. R., & Kerr, J. N. (2008). Population imaging of ongoing neuronal activity in the visual cortex of awake rats. *Nature Neuroscience, 11,* 749–751. [PubMed]

Grinvald, A., Lieke, E., Frostig, R. D., Gilbert, C. D., & Wiesel, T. N. (1986). Functional architecture of cortex revealed by optical imaging of intrinsic signals. *Nature, 324,* 361–364. [PubMed]

Hashemi-Nezhad, M., Blessing, E. M., Dreher, B., & Martin, P. R. (2008). Segregation of short-wavelength sensitive ("blue") cone signals among neurons in the lateral geniculate nucleus and striate cortex of marmosets. *Vision Research*. [PubMed]

Hendry, S. H., & Reid, R. C. (2000). The koniocellular pathway in primate vision. *Annual Review of Neuroscience, 23,* 127–153. [PubMed]

Hendry, S. H., & Yoshioka, T. (1994). A neurochemically distinct third channel in the macaque dorsal lateral geniculate nucleus. *Science, 264,* 575–577. [PubMed]

Horton, J. C., & Hubel, D. H. (1981). A regular patchy distribution of cytochrome-oxidase staining in primary visual cortex of the macaque monkey. *Nature, 292,* 762–764. [PubMed]

Horwitz, G. D., Chichilnisky, E. J., & Albright, T. D. (2005). Blue-yellow signals are enhanced by spatiotemporal luminance contrast in macaque V1. *Journal of Neurophysiology, 93,* 2263–2278. [PubMed] [Article]

Hubel, D., & Livingstone, M. (1990). Color puzzles. *Cold Spring Harbor Symposia on Quantitative Biology, 55,* 643–649. [PubMed]

Jacobs, G. H. (1993). The distribution and nature of colour vision among the mammals. *Biological Reviews, 68,* 413–471. [PubMed]

Johnson, E. N., Hawken, M. J., & Shapley, R. (2004). Cone inputs in macaque primary visual cortex. *Journal of Neurophysiology, 91,* 2501–2514. [PubMed] [Article]

Kremers, J., Weiss, S., Zrenner, E., & Maurer, J. (1997). Spectral responsivity of lateral geniculate cells in the dichromatic common marmoset (*Callithrix jacchus*). Rod and cone inputs to parvo- and magnocellular cells. In C. R. Cavonius (Ed.), *Colour vision deficiencies XIII* (pp. 87–97). Dordrecht: Kluwer Academic Publishers.

Lachica, E. A., & Casagrande, V. A. (1992). Direct W-like geniculate projections to the cytochrome oxidase (CO) blobs in primate visual cortex: Axon morphology. *Journal of Comparative Neurology, 319,* 141–158. [PubMed]

Landisman, C. E., & Ts'o, D. Y. (2002a). Color processing in macaque striate cortex: Electrophysiological properties. *Journal of Neurophysiology, 87,* 3138–3151. [PubMed] [Article]

Landisman, C. E., & Ts'o, D. Y. (2002b). Color processing in macaque striate cortex: Relationships to ocular dominance, cytochrome oxidase, and orientation. *Journal of Neurophysiology, 87,* 3126–3137. [PubMed] [Article]

Lee, B. B., Valberg, A., Tigwell, D. A., & Tryti, J. (1987). An account of responses of spectrally opponent neurons in macaque lateral geniculate nucleus to successive contrast. *Proceedings of the Royal Society of London B: Biological Sciences, 230,* 293–314. [PubMed]

Leventhal, A. G., Thompson, K. G., Liu, D., Zhou, Y., & Ault, S. J. (1995). Concomitant sensitivity to orientation, direction, and color of cells in layers 2, 3, and 4 of monkey striate cortex. *Journal of Neuroscience, 15,* 1808–1818. [PubMed] [Article]

Livingstone, M. S., & Hubel, D. H. (1982). Thalamic inputs to cytochrome oxidase-rich regions in monkey visual cortex. *Proceedings of the National Academy of Sciences of the United States of America, 79,* 6098–6101. [PubMed] [Article]

Livingstone, M. S., & Hubel, D. H. (1984). Anatomy and physiology of a color system in the primate visual cortex. *Journal of Neuroscience, 4,* 309–356. [PubMed] [Article]

Lu, H. D., & Roe, A. W. (2007). Optical imaging of contrast response in macaque monkey V1 and V2. *Cerebral Cortex, 17,* 2675–2695. [PubMed] [Article]

Lu, H. D., & Roe, A. W. (2008). Functional organization of color domains in V1 and V2 of Macaque monkey revealed by optical imaging. *Cerebral Cortex, 18,* 516–533. [PubMed] [Article]

Malonek, D., Dirnagl, U., Lindauer, U., Yamada, K., Kanno, I., & Grinvald, A. (1997). Vascular imprints of neuronal activity: Relationships between the dynamics of cortical blood flow, oxygenation, and volume changes following sensory stimulation.

Proceedings of the National Academy of Sciences of the United States of America, 94, 14826–14831. [PubMed] [Article]

Markstahler, U., Bach, M., & Spatz, W. B. (1998). Transient molecular visualization of ocular dominance columns (ODCs) in normal adult marmosets despite the desegregated termination of the retinogeniculo-cortical pathways. *Journal of Comparative Neurology, 393,* 118–134. [PubMed]

Martin, P. R., White, A. J., Goodchild, A. K., Wilder, H. D., & Sefton, A. E. (1997). Evidence that blue-on cells are part of the third geniculocortical pathway in primates. *European Journal of Neuroscience, 9,* 1536–1541. [PubMed]

Mayhew, J. E., Askew, S., Zheng, Y., Porrill, J., Westby, G. W., Redgrave, P., et al. (1996). Cerebral vasomotion: A 0.1-Hz oscillation in reflected light imaging of neural activity. *Neuroimage, 4,* 183–193. [PubMed]

McLoughlin, N., & Schiessl, I. (2006). Orientation selectivity in the common marmoset (*Callithrix jacchus*): The periodicity of orientation columns in V1 and V2. *Neuroimage, 31,* 76–85. [PubMed]

Mechler, F., & Ringach, D. L. (2002). On the classification of simple and complex cells. *Vision Research, 42,* 1017–1033. [PubMed]

Meister, M., & Bonhoeffer, T. (2001). Tuning and topography in an odor map on the rat olfactory bulb. *Journal of Neuroscience, 21,* 1351–1360. [PubMed] [Article]

Mollon, J. D. (1989). "Tho' she kneel'd in the place where they grew." The uses and origins of primate colour vision. *Journal of Experimental Biology, 146,* 21–38. [PubMed] [Article]

Naka, K. I., & Rushton, W. A. (1966). S-potentials from colour units in the retina of fish (*Cyprinidae*). *The Journal of Physiology, 185,* 536–555. [PubMed] [Article]

Nathans, J. (1999). The evolution and physiology of human color vision: Insights from molecular genetic studies of visual pigments. *Neuron, 24,* 299–312. [PubMed] [Article]

Roe, A. W., Fritsches, K., & Pettigrew, J. D. (2005). Optical imaging of functional organization of V1 and V2 in marmoset visual cortex. *Anatomical Record, 287,* 1213–1225. [PubMed]

Roe, A. W., & Ts'o, D. Y. (1999). Specificity of color connectivity between primate V1 and V2. *Journal of Neurophysiology, 82,* 2719–2730. [PubMed] [Article]

Sato, H., Katsuyama, N., Tamura, H., Hata, Y., & Tsumoto, T. (1994). Broad-tuned chromatic inputs to color-selective neurons in the monkey visual cortex. *Journal of Neurophysiology, 72,* 163–168. [PubMed]

Sceniak, M. P., Ringach, D. L., Hawken, M. J., & Shapley, R. (1999). Contrast's effect on spatial summation by macaque V1 neurons. *Nature Neuroscience, 2,* 733–739. [PubMed]

Schiessl, I., & McLoughlin, N. (2003). Optical imaging of the retinotopic organization of V1 in the common marmoset. *Neuroimage, 20,* 1857–1864. [PubMed]

Sengpiel, F., Troilo, D., Kind, P. C., Graham, B., & Blakemore, C. (1996). Functional architecture of area 17 in normal and monocularly deprived marmosets (*Callithrix jacchus*). *Visual Neuroscience, 13,* 145–160. [PubMed]

Sincich, L. C., & Horton, J. C. (2005). The circuitry of V1 and V2: Integration of color, form, and motion. *Annual Review of Neuroscience, 28,* 303–326. [PubMed]

Skottun, B. C., De Valois, R. L., Grosof, D. H., Movshon, J. A., Albrecht, D. G., & Bonds, A. B. (1991). Classifying simple and complex cells on the basis of response modulation. *Vision Research, 31,* 1079–1086. [PubMed]

Solomon, S. G. (2002). Striate cortex in dichromatic and trichromatic marmosets: Neurochemical compartmentalization and geniculate input. *Journal of Comparative Neurology, 450,* 366–381. [PubMed]

Solomon, S. G., & Lennie, P. (2005). Chromatic gain controls in visual cortical neurons. *Journal of Neuroscience, 25,* 4779–4792. [PubMed] [Article]

Solomon, S. G., White, A. J., & Martin, P. R. (1999). Temporal contrast sensitivity in the lateral geniculate nucleus of a New World monkey, the marmoset *Callithrix jacchus*. *The Journal of Physiology, 517,* 907–917. [PubMed] [Article]

Spatz, W. B. (1989). Loss of ocular dominance columns with maturity in the monkey, *Callithrix jacchus*. *Brain Research, 488,* 376–380. [PubMed]

Spatz, W. B., Illing, R. B., & Weisenhorn, D. M. (1994). Distribution of cytochrome oxidase and parvalbumin in the primary visual cortex of the adult and neonate monkey, *Callithrix jacchus*. *Journal of Comparative Neurology, 339,* 519–534. [PubMed]

Sun, H., Smithson, H. E., Zaidi, Q., & Lee, B. B. (2006). Specificity of cone inputs to macaque retinal ganglion cells. *Journal of Neurophysiology, 95,* 837–849. [PubMed] [Article]

Szmajda, B. A., Buzás, P., Fitzgibbon, T., & Martin, P. R. (2006). Geniculocortical relay of blue-off signals in the primate visual system. *Proceedings of the National Academy of Sciences of the United States of America, 103,* 19512–19517. [PubMed] [Article]

Tootell, R. B., Nelissen, K., Vanduffel, W., & Orban, G. A. (2004). Search for color 'center(s)' in macaque visual cortex. *Cerebral Cortex, 14,* 353–363. [PubMed] [Article]

Tootell, R. B., Silverman, M. S., Hamilton, S. L., De Valois, R. L., & Switkes, E. (1988). Functional anatomy of macaque striate cortex. III. Color. *Journal of Neuroscience, 8,* 1569–1593. [PubMed] [Article]

Tovée, M. J., Bowmaker, J. K., & Mollon, J. D. (1992). The relationship between cone pigments and behavioural sensitivity in a New World monkey (*Callithrix jacchus jacchus*). *Vision Research, 32,* 867–878. [PubMed]

Travis, D. S., Bowmaker, J. K., & Mollon, J. D. (1988). Polymorphism of visual pigments in a callitrichid monkey. *Vision Research, 28,* 481–490. [PubMed]

Troilo, D., Howland, H. C., & Judge, S. J. (1993). Visual optics and retinal cone topography in the common marmoset (*Callithrix jacchus*). *Vision Research, 33,* 1301–1310. [PubMed]

Ts'o, D. Y., & Gilbert, C. D. (1988). The organization of chromatic and spatial interactions in the primate striate cortex. *Journal of Neuroscience, 8,* 1712–1727. [PubMed] [Article]

Vanzetta, I., Hildesheim, R., & Grinvald, A. (2005). Compartment-resolved imaging of activity-dependent dynamics of cortical blood volume and oximetry. *Journal of Neuroscience, 25,* 2233–2244. [PubMed] [Article]

Victor, J. D., Blessing, E. M., Forte, J. D., Buzás, P., & Martin, P. R. (2007). Response variability of marmoset parvocellular neurons. *The Journal of Physiology, 579,* 29–51. [PubMed] [Article]

Viswanathan, A., & Freeman, R. D. (2007). Neurometabolic coupling in cerebral cortex reflects synaptic more than spiking activity. *Nature Neuroscience, 10,* 1308–1312. [PubMed]

White, A. J., Solomon, S. G., & Martin, P. R. (2001). Spatial properties of koniocellular cells in the lateral geniculate nucleus of the marmoset *Callithrix jacchus*. *The Journal of Physiology, 533,* 519–535. [PubMed] [Article]

Wong-Riley, M. (1979). Changes in the visual system of monocularly sutured or enucleated cats demonstrable with cytochrome oxidase histochemisty. *Brain Research, 171,* 11–28. [PubMed]

Xiao, Y., Casti, A., Xiao, J., & Kaplan, E. (2007). Hue maps in primate striate cortex. *Neuroimage, 35,* 771–786. [PubMed] [Article]

Xu, X., Bosking, W., Sáry, G., Stefansic, J., Shima, D., & Casagrande, V. (2004). Functional organization of visual cortex in the owl monkey. *Journal of Neuroscience, 24,* 6237–6247. [PubMed] [Article]

Xu, X., Ichida, J. M., Allison, J. D., Boyd, J. D., Bonds, A. B., & Casagrande, V. A. (2001). A comparison of koniocellular, magnocellular and parvocellular receptive field properties in the lateral geniculate nucleus of the owl monkey (*Aotus trivirgatus*). *The Journal of Physiology, 531,* 203–218. [PubMed] [Article]

Yeh, T., Lee, B. B., Kremers, J., Cowing, J. A., Hunt, D. M., Martin, P. R., et al. (1995). Visual responses in the lateral geniculate nucleus of dichromatic and trichromatic marmosets (*Callithrix jacchus*). *Journal of Neuroscience, 15,* 7892–7904. [PubMed] [Article]

Yoshioka, T., Blasdel, G. G., Levitt, J. B., & Lund, J. S. (1996). Relation between patterns of intrinsic lateral connectivity, ocular dominance, and cytochrome oxidase-reactive regions in macaque monkey striate cortex. *Cerebral Cortex, 6,* 297–310. [PubMed] [Article]

Yoshioka, T., & Dow, B. M. (1996). Color, orientation and cytochrome oxidase reactivity in areas V1, V2 and V4 of macaque monkey visual cortex. *Behavioural Brain Research, 76,* 71–88. [PubMed]